

CFD Prediction of Tandem Water Columns Aerobreakup Using Open-Source Codes

F. Edoardo Taglialatela(✉) and Giuliano De Stefano

Engineering Department, University of Campania Luigi Vanvitelli, 81031 Aversa, Italy
feliceedoardo.taglialatela@unicampania.it

Abstract. The present study addresses the comparison of two different novel open-source computational fluid dynamics (CFD) codes for the numerical simulation of the deformation and breakup of tandem water columns subjected to high-speed air flow. The computations are conducted using the code ECOGEN and a customized version of OpenFOAM. Both codes employ a volume-of-fluid interface-tracking method coupled with a higher-order finite-volume approach. Unlike some similar studies, viscous and capillary effects are taken into account. As to the computational setup, a virtual shock tube environment is arranged to accurately replicate the experimental conditions. The well-defined post-shock air flow conditions allow to model the post-impact dynamics, capturing key phenomena such as interface deformation, leading edge drift, and incipient breakup. A comparative analysis of the results highlights the strengths and limitations of each solver. Comparison of results with experimental observations indicates that while both codes capture the primary mechanism of aerobreakup, differences arise in the formation of early-stage instabilities and ligament stripping dynamics. By validating open-source codes against experimental observations, this study aims to contribute to the ongoing refinement of multiphase flow modeling tools.

Keywords: Multiphase flow · compressible flow · aerobreakup · computational fluid dynamics

1 Introduction

Aerobreakup is a highly widespread phenomenon, frequently occurring in nature (e.g., in raindrops formation) as well as in industrial engineering applications. To name but a few, one can consider combustion and detonation of multiphase mixture [1], and erosion damage to structures [2,3]. Droplet *aerobreakup* happens when a high-velocity air stream impacts a liquid droplet. The liquid body, due to the surrounding gas flow, experiences significant deformation and subsequent fragmentation into a multitude of smaller sub-droplets, referred to as *daughter* droplets. During the interaction, the momentum transport from the high-speed air flow and the resistive forces, caused by both surface tension and viscosity,

© The Author(s), under exclusive license to Springer Nature Switzerland AG 2025
O. Gervasi et al. (Eds.): ICCSA 2025, LNCS 15648, pp. 36–50, 2025.
https://doi.org/10.1007/978-3-031-97000-9_3

oppose each other. The imbalance between the two determines the degree of deformation. For this reason, the physical mechanism can be cataloged in terms of two non-dimensional parameters, namely, the Weber number

$$\mathrm{We} = \frac{\rho_{\mathrm{g}} u_{\mathrm{g}}^2 \mathrm{d}_0}{\sigma} \tag{1}$$

that relates aerodynamic forces and surface tension forces, and the Ohnesorge number

$$\mathrm{Oh} = \frac{\mu_\ell}{\sqrt{\rho_\ell \sigma \mathrm{d}_0}} \tag{2}$$

that compares the viscosity of the liquid and surface tension effects. Here, ρ and u_g are the post shock density and velocity magnitude, d_0 is the initial droplet diameter, μ is the viscosity and σ is the surface tension coefficient between the two different fluids. The subscripts "ℓ" and "g" denote the liquid and gas phase, respectively.

The Weber number is a key parameter to catalog the breakup regimes, not only to embed the main physical features of the phenomenon, but also to determine the characteristics of the resultant droplet cloud. The original classification involved five distinct regimes: *vibrational breakup*, *bag breakup*, *multimode breakup*, *sheet thinning breakup* and *catastrophic breakup*. Each of them occurred in specific ranges of the Weber number. More recently, Theofanous and Li [4,5] provided a complete review of aerobreakup physics, and a new classification. In particular, it was recognized that the so-called *catastrophic breakup* regime was only a visual artifact observed in the experiments. The re-classification consists of only two distinct regimes: the Rayleigh-Taylor Piercing (RTP) is observed for $10 < \mathrm{We} < 10^2$, and the Shear-Induced Entrainment (SIE) occurred for $\mathrm{We} > 10^3$. At low Weber number, the primary factor inducing breakup are Rayleigh-Taylor instabilities, whereas at higher Weber number, the predominant mechanism for liquid filament stripping is attributed to the substantial shear effects exerted by the adjacent airflow. As the relative importance of viscous forces is expressed by the Ohnesorge number, it is that for low values of this parameter ($\mathrm{Oh} < 0.1$), the viscosity plays a very marginal role, and can be neglected. On the other hand, at higher values ($\mathrm{Oh} > 1$), the required forces for the breakup increase owing to viscous dissipation, e.g. [6].

The primary objective of the study is to set up a virtual shock tube environment using two different open-source codes based on the finite volume (FV) approach. The two codes employed are ECOGEN [7] and a custom version of OpenFOAM using the solver vofTwoPhaseCentralFoam [8]. The first was developed by Schmidmayer et al. [9], while the second was introduced by Kraposhin and co-workers [10]. Both solvers were successfully tested for multidimensional compressible single-phase and two-phase flows, e.g. 1D and 2D transport tests, surface tension tests to verify Laplace's law, gas-liquid shock tube and other significant problems [9,10]. Performance scalability tests have also been provided.

In this study, the tandem breakup phenomenon is investigated in order to effectively predict the post-shock droplet dynamics, in terms of leading edge drift and streamwise extent. Also, a qualitative view of the flow field and the overall

interface deformation dynamics of the two cylinders is shown. Differently from previous droplet aerobreakup studies following the unsteady Reynolds-averaged Navier-Stokes (URANS) approach [11–13], where the mean flow was resolved, supplying the simulation with suitable turbulence closures, the present codes directly solve the original governing equations. However, in contrast to other scale-resolving simulations [14,15], the current methods do not utilize an explicit subgrid-scale model for approximating the effect of unresolved turbulent flow motions. Rather, they rely on the implicit numerical dissipation provided by the adopted numerical scheme, e.g. [16].

The residual of the paper is organized as follows. In Sect. 2, the physical model of the problem is introduced, including the governing equations for both solvers. The CFD models are described in Sect. 3, while the results of the numerical computations are presented and discussed in Sect. 4. Finally, some concluding remarks are drawn in Sect. 5.

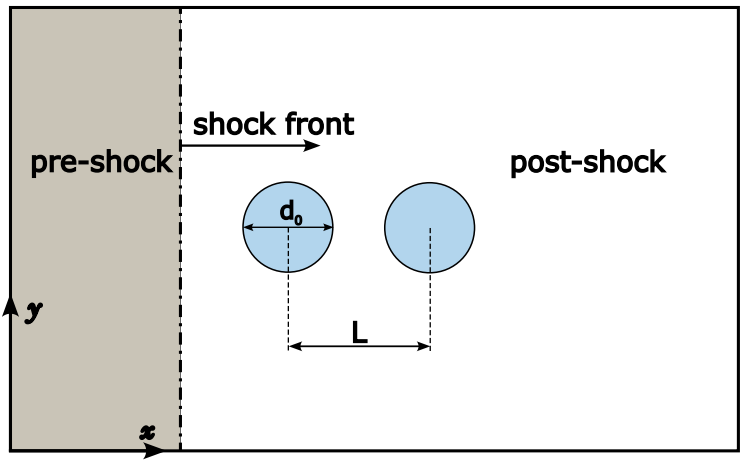

Fig. 1. Two-phase flow geometry (not in scale).

2 Physical Model

The shock/droplet interaction is often studied in two dimensions by simulating the shock wave passage over a water column, e.g. [11]. Pioneering experimental studies such as those by Igra and Takayama [17,18] are generally used to verify numerical results. A very common experimental setup is represented by a shock tube, where a physical diaphragm divides the enclosed tube into two distinct zones: a driver section with high-pressure air and a driven section at atmospheric conditions. Once the diaphragm is removed, a travelling shock is produced that impacts the column in the test zone. The described setup aims to

produce very well-defined post-shock conditions for the water bodies. Figure 1 shows the domain of the problem, where two cylinders with diameter d_0 are situated in the driven section at the distance L.

In the following subsections, the systems of equations used by ECOGEN and vofTwoPhaseCentralFoam are presented, for the specific case of a liquid-gas mixture. Both methods are derived from the Baer-Nunziato 7-equation model [19] and combine a volume-of-fluid (VOF) interface-capturing scheme with a shock-capturing FV approach. Furthermore, both are influenced by a parameter represented as μ, referred to as pressure relaxation coefficient, which determines the speed at which the system attains mechanical equilibrium.

2.1 ECOGEN: Six-Equation Model

The six-equation model should not be considered as a physical model, but more as a step model to numerically solve the equations upon using a finite or infinite pressure relaxation. The better properties for the numerical approximation regard the preservation of the positivity for the volume fractions and the monotonicity of sound speed. The pressure- and temperature-disequilibrium, multicomponent system of equations employed by ECOGEN is the following [20]:

$$\frac{\partial \alpha_\ell}{\partial t} + \boldsymbol{u} \cdot \nabla \alpha_\ell = \mu(p_\ell - p_\mathrm{g}), \tag{3}$$

$$\frac{\partial \alpha_\ell \rho_\ell}{\partial t} + \nabla \cdot (\alpha_\ell \rho_\ell \boldsymbol{u}) = 0, \tag{4}$$

$$\frac{\partial \alpha_\mathrm{g} \rho_\mathrm{g}}{\partial t} + \nabla \cdot (\alpha_\mathrm{g} \rho_\mathrm{g} \boldsymbol{u}) = 0, \tag{5}$$

$$\frac{\partial \rho \boldsymbol{u}}{\partial t} + \nabla \cdot (\rho \boldsymbol{u} \otimes \boldsymbol{u} + p\boldsymbol{I} + \boldsymbol{\Omega} - \boldsymbol{\tau}) = \boldsymbol{0}, \tag{6}$$

$$\frac{\partial \alpha_\ell \rho_\ell e_\ell}{\partial t} + \nabla \cdot (\alpha_\ell \rho_\ell e_\ell \boldsymbol{u}) + \alpha_\ell p_\ell \nabla \cdot \boldsymbol{u} = -p_I \mu (p_\ell - p_\mathrm{g}) + \alpha_\ell \boldsymbol{\tau}_\ell : \boldsymbol{\nabla u}, \tag{7}$$

$$\frac{\partial \alpha_\mathrm{g} \rho_\mathrm{g} e_\mathrm{g}}{\partial t} + \nabla \cdot (\alpha_\mathrm{g} \rho_\mathrm{g} e_\mathrm{g} \boldsymbol{u}) + \alpha_\mathrm{g} p_\mathrm{g} \nabla \cdot \boldsymbol{u} = p_I \mu (p_\ell - p_\mathrm{g}) + \alpha_g \boldsymbol{\tau}_\mathrm{g} : \boldsymbol{\nabla u}. \tag{8}$$

In the above equations: μ represents the relaxation parameter; α_k, ρ_k, e_k, and p_k indicate volume fraction, density, internal energy, and pressure of one of the two components ($k = \ell$ or $k = \mathrm{g}$); $\boldsymbol{I}$ stands for the identity tensor; the variable $p_I = \frac{Z_\mathrm{g} p_\ell + Z_\ell p_\mathrm{g}}{Z_\ell + Z_\mathrm{g}}$ denotes the interfacial pressure; $Z_k = \rho_k c_k$ the acoustic impedance; $\boldsymbol{\Omega}$ is the capillary tensor; $\boldsymbol{\tau}$ is the viscous stress tensor. In the VOF formulation, the mixture variables are given by

$$\rho = \alpha_\ell \rho_\ell + \alpha_\mathrm{g} \rho_\mathrm{g} \quad \text{and} \quad p = \alpha_\ell p_\ell + \alpha_\mathrm{g} p_\mathrm{g}. \tag{9}$$

In regular zones the model is self-consistent. However, in presence of shocks, the internal energy equations are inappropriate because of their non-conservative nature. Due to this reason, a redundant equation for the total energy of the

mixture is necessary to correct the thermodynamic state predicted [21]. The equation reads:

$$\frac{\partial \rho E + \varepsilon_\sigma}{\partial t} + \nabla \cdot ((\rho E + \varepsilon_\sigma + p)\boldsymbol{u} + \boldsymbol{\Omega} \cdot \boldsymbol{u} - \boldsymbol{\tau} \cdot \boldsymbol{u}) = 0, \tag{10}$$

where $E = e + \frac{1}{2}\|\boldsymbol{u}\|^2$, and ε_σ is the capillary energy. The internal energy is given by

$$e = Y_\ell e_\ell + Y_\mathrm{g} e_\mathrm{g}. \tag{11}$$

In this equation, $Y_k = \frac{\alpha_k \rho_k}{\rho}$ are the mass fractions, and e_k is given by an appropriate equation of state.

In this case, finite relaxation is used and the value of 3.5 is selected for the parameter μ, which plays a crucial role [22].

2.2 vofTwoPhaseCentralFoam: Five-Equation Model

The infinite pressure relaxation hypothesis ($\mu \to +\infty$), meaning that the equilibrium state is reached instantly, makes the six-equation model converge to the mechanical-equilibrium model of Kapila et al. [23]. At the end of the asymptotic reduction process [21], there exists a single equilibrium pressure (and velocity), suppressing undesired spurious interfacial oscillations. The resulting hyperbolic model is thermodynamically consistent and particularly suitable for describing immiscible fluids. In the case of a water-air mixture, it reads [24]:

$$\frac{\partial \rho}{\partial t} + \boldsymbol{\nabla} \cdot (\rho \boldsymbol{u}) = 0, \tag{12}$$

$$\frac{\partial (\rho \boldsymbol{u})}{\partial t} + \boldsymbol{\nabla} \cdot (\rho \boldsymbol{u} \otimes \boldsymbol{u}) = -\nabla p + \boldsymbol{\nabla} \cdot \boldsymbol{\tau}, \tag{13}$$

$$\frac{\partial (\rho E)}{\partial t} + \boldsymbol{\nabla} \cdot [(\rho E + p)\boldsymbol{u}] = \boldsymbol{\nabla} \cdot (\boldsymbol{\tau} \cdot \boldsymbol{u}), \tag{14}$$

$$\frac{\partial (\alpha_\ell \rho_\ell)}{\partial t} + \boldsymbol{\nabla} \cdot (\alpha_\ell \rho_\ell \boldsymbol{u}) = 0, \tag{15}$$

$$\frac{\partial \alpha_\ell}{\partial t} + \boldsymbol{\nabla} \cdot (\alpha_\ell \boldsymbol{u}) = \alpha_\ell \boldsymbol{\nabla} \cdot \boldsymbol{u} + K \boldsymbol{\nabla} \cdot \boldsymbol{u}, \tag{16}$$

where $K = \frac{\alpha_\ell \alpha_\mathrm{g} (Z_\ell - Z_\mathrm{g})}{\alpha_\ell Z_\ell + \alpha_\mathrm{g} Z_\mathrm{g}}$ is the interface compression coefficient, while the other symbols represent the same quantities already defined in Sect. 2.1.

2.3 Thermodynamic Closure

As far as the thermodynamic closure is concerned, both CFD models treat the air phase as an ideal gas. By denoting $\mathrm{R_g} = \mathrm{R}/\mathrm{M_g}$ the particular gas constant,

with M_g the associated molar mass, and R the universal gas constant, the gas density is calculated as follows:

$$\rho_g = \frac{p_g}{R_g T}. \tag{17}$$

As for the water phase, ECOGEN uses the stiffened equation of state, thus the density is:

$$\rho_\ell = \frac{p_\ell + \pi_\infty}{(e_\ell - e_{\ell,\mathrm{ref}})(\gamma_{sg} - 1)}, \tag{18}$$

where π_∞ and γ_{sg} are fitting parameters set according to [25]. Table 1 sums up the properties of the fluids used in the current simulations.

Table 1. Fluids properties.

Parameter	Description	Value	Unit
ρ_ℓ	Liquid density	1028	$kg \cdot m^{-3}$
π_∞	SG fitting parameter	343.44	MPa
γ_{sg}	SG fitting parameter	6.12	–
σ	Surface tension	0.0728	$N \cdot m^{-1}$
μ_ℓ	Liquid dynamic viscosity	1.0×10^{-3}	$Pa \cdot s$
μ_g	Gas dynamic viscosity	1.85×10^{-5}	$Pa \cdot s$

On the other hand, the equation of state for water in vofTwoPhaseCentralFoam corresponds to the perfect fluid formulation, calculating the density as follows:

$$\rho_\ell = \rho_{\ell 0} + \frac{p}{RT}. \tag{19}$$

Following experimental studies, the initial diameter d_0 is set to 4.8mm and the center-to-center distance between the columns, L, is 30mm [18]. In addition, given the properties in Table 1, the non-dimensional numbers defined in Eq. 1 and Eq. 2 are: $We = 7.41 \times 10^3$ and $Oh = 1.70 \times 10^{-3}$. The Reynolds number is $Re = 1.07 \times 10^5$. These conditions place the phenomenon in the SIE regime, as confirmed by [4]. Lastly, owing to the low Oh number, capillary effects could be neglected, as in previous studies [25]. However, in the present simulations, those effects are included, as they become more important in the late stages of the interaction [26,27].

3 Computational Models

Using the initial column diameter d_0 as a reference length, the computational domain Ω is measured as a multiple of it. In both simulations, Ω is initialized

to reproduce the experimental conditions of the shock tube and to simulate the interaction in its entirety, without enforcing any symmetry. Given the Mach number of the shock, the compression ratio $\beta = p_2/p_1$ is known and can be used to obtain p_4/p_1, where the subscripts "4" and "1" are used to denote driver and driven sections, respectively. The two sections, separated by a virtual diaphragm, are initialized with still air ($u_4 = u_1 = 0$) at the same temperature ($T_4 = T_1$) and very different pressure and density levels: $p_4 \gg p_1$, $\rho_4 \gg \rho_1$. The cell size of was chosen according to previous studies, decreasing it compared to [25,28].

3.1 Code ECOGEN

In the above context, the physical domain shown in Fig. 1 is discretized using a structured grid made up entirely of square cells. The novel adaptive mesh refinement (AMR) technique presented in [29] is used, refining the grid twice based on the gradients of the field variables in the domain. The finest resolution is 128 cells per diameter (cpd). The non-reflective boundary conditions (NRBCs) are set to every boundary and allow to shrink the domain without unphysical reflections influencing the test zone. The final dimensions for Ω are $[0, 25\mathrm{d}_0] \times [0, 10\mathrm{d}_0]$.

The numerical solution of equations (3) to (8) is structured as follows, and it is based on a splitting procedure:

- the left-hand side of the equations are solved using an explicit Godunov-type method, where it is included the additional equation for the energy correction;
- the relaxation terms are integrated with a first-order explicit Euler scheme;
- a second-order monotonic upwind scheme for conservation laws (MUSCL) is used, where a monotonized central (MC) limiter is employed for the primitive variables;
- the timestep is automatically controlled to maintain the Courant-Friedrich-Levy (CFL) number below 0.6.

For further information regarding the model, the interested reader is encouraged to delve into the articles detailing the solution method, i.e. [20].

3.2 Code vofTwoPhaseCentralFoam

The computational domain used to obtain the solution in OpenFOAM is divided into a uniform square grid. In the absence of AMR, to obtain a higher resolution where needed, multiple nested refinement regions are programmed to gradually increase the local resolution. The finest region is made of 128 cpd. The domain itself is much larger, compared to the one used in ECOGEN, measuring $\Omega = [-24\mathrm{d}_0, 96\mathrm{d}_0] \times [-30\mathrm{d}_0, 30\mathrm{d}_0]$. With such an extent, the absence of NRBCs and the subsequent unphysical reflections do not interfere with the simulation, allowing for longer visualization times. The boundary conditions applied are shown in Table 2, using the OpenFOAM naming convention. Here, the solving procedure is as follows:

- fluxes are calculated using a hybrid Kurganov-Noelle-Petrova (KNP)/ PIMPLE algorithm, to ensure monotonicity of the primitive variables;
- the acoustically conservative interface discretization (ACID) technique helps suppress spurious oscillations near the interfaces;
- the multidimensional universal limiter for explicit solution (MULES) approach is used, where a Minmod limiter is employed;
- the equations are marched in time using a first-order explicit Euler scheme;
- the timestep is automatically controlled setting CFL < 0.15.

Figure 2 shows the comparison of both meshes in proximity to the water body. For further information on the numerical model, the interested reader is encouraged to consult [10]. In addition, more details on the implementation of this particular solver for the investigation of droplet aerobreakup can be found in [30].

Table 2. Summary of boundary conditions employed in the OpenFOAM solver.

Boundary	p	T	$\boldsymbol{u}$	α_ℓ
Driver section side	zeroGradient	zeroGradient	fixedValue	fixedValue
Driven section side	zeroGradient	zeroGradient	zeroGradient	zeroGradient
Lateral sides	zeroGradient	zeroGradient	slip	zeroGradient

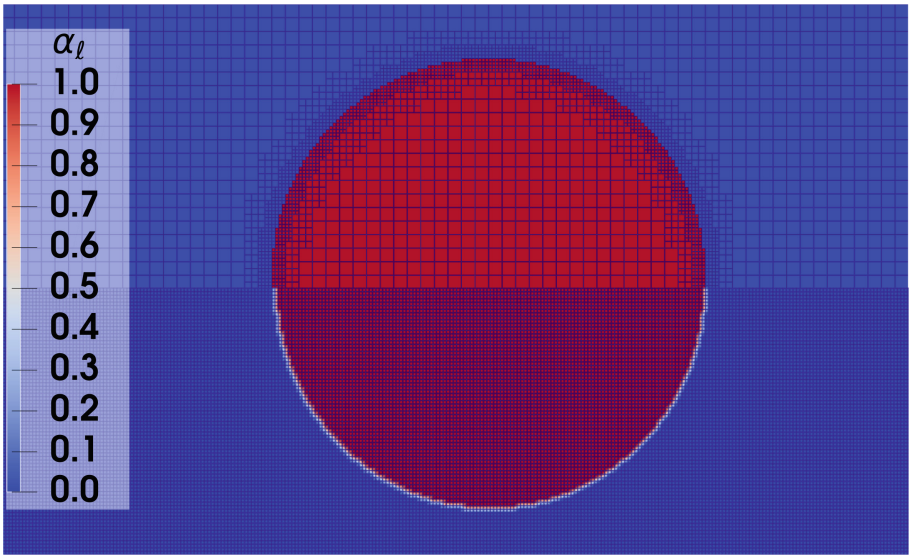

Fig. 2. Comparison between the meshes: ECOGEN (top) and vofTwoPhaseCentralFoam (bottom).

4 Results

Both solutions are analyzed from a qualitative point of view, depicting the velocity magnitude and the numerical Schlieren contours shown in Fig. 3. Herein, the numerical Schlieren is defined by:

$$\Phi = \exp\left(-\mathrm{k}\frac{|\nabla\rho|}{\max(|\nabla\rho|)}\right), \tag{20}$$

where k is a user-defined constant.

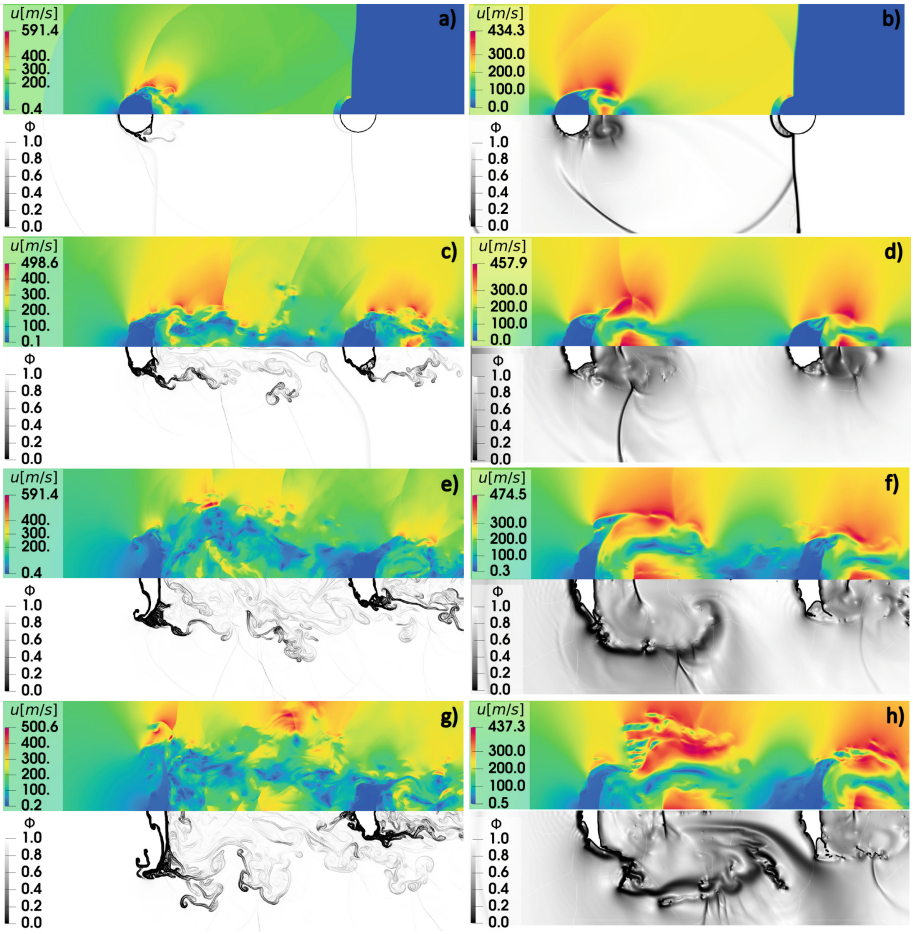

Fig. 3. Velocity magnitude and Schlieren contours for ECOGEN (left) and vofTwoPhaseCentralFoam (right) at $t^* \approx 3.1$, 9, 15.1, and 17.9.

Notably, the calculated velocity magnitudes are different: ECOGEN predicts higher peak values, localized further from the interface. The pressure differen-

tial between the two sides of each cylinder is captured by both codes, which eventually causes flattening and peripheral elongation.

Figure 4 shows the time histories of the volume fraction contour of the liquid phase, sampled for both solvers. It can be seen that the time evolution of the captured interface is similar in the early stages, and as time passes, more differences arise. The aforementioned flattening shows itself in both simulations. However, a first difference can be seen on the front side, where vofTwoPhaseCentralFoam captures more instabilities, while the other solution appears to be more regular (details in Figs. 4 (a) and 4 (b)).

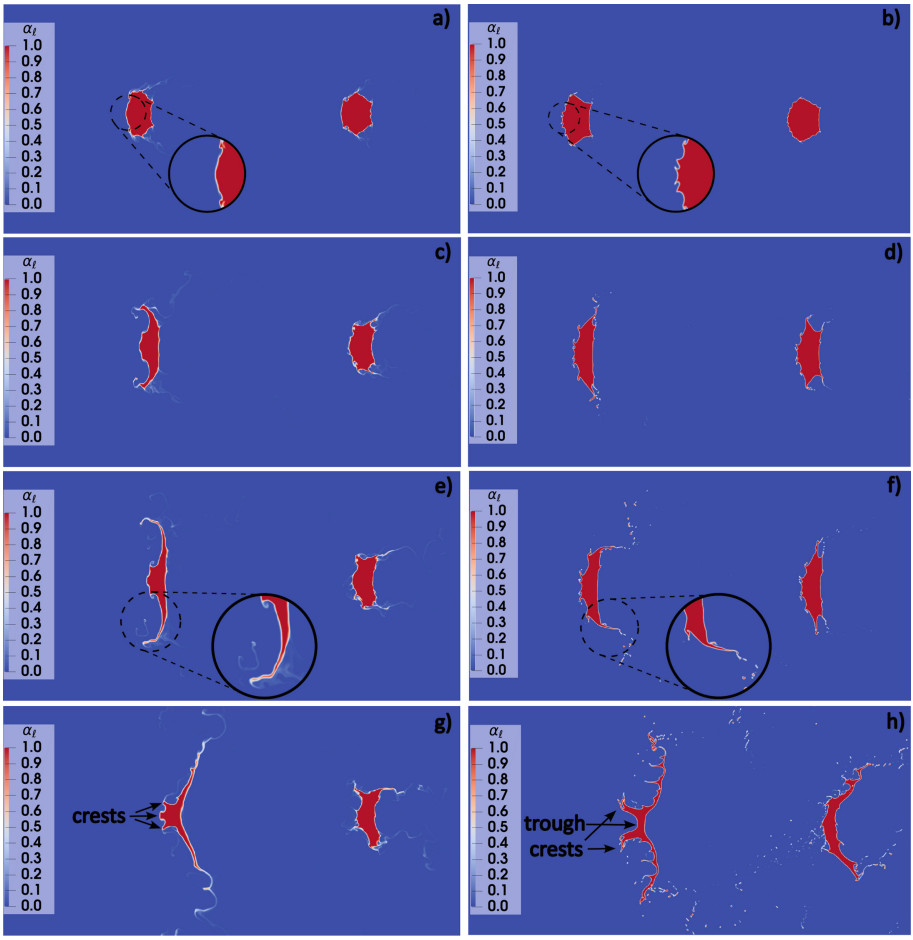

Fig. 4. Liquid volume fraction contours for ECOGEN (left) and vofTwoPhaseCentralFoam (right) at $t^* \approx 9$, 15.1, 17.9 and 22.1 (from top to bottom row).

According to experimental findings, the early stages of the interaction show a closer match with what was calculated by ECOGEN. In fact, as mentioned by

Theofanous and Li in [4], a significant area surrounding the front stagnation point is smooth, while the radially redirected flow gives birth to surface instabilities that produce peripheral elongation and ultimately lips. This characteristic of mass redistribution from a cylinder to an elongated structure also aligns with what was observed in the SIE regime, where the stripping mechanism drives the fragmentation.

In the above context, the prediction of the lips highlights a different behavior. As shown in the particulars of Fig. 4 (e) and Fig. 4 (f), the ligaments predicted by vofTwoPhaseCentralFoam tend to go downstream, while the more peripheral and diffuse parts calculated by ECOGEN initially point in the opposite direction. As time passes, the vofTwoPhaseCentralFoam calculation resembles the formation of the ligaments and the overall shape of the cylinders more closely [4,27,31]. In the late stages, ECOGEN recovers the correct behavior, as the shedded lips are pushed by the air stream toward the leeward side (subfigures (g) and (h)), and the two captured surfaces appear similar. Connected with the late stages, the prediction of the front stagnation zone is similar: both simulations show that the surface instabilities previously created tend to drift less, when compared to the rest of the cylinder, which gets further pushed downstream.

With respect to the rear column, both solutions show similar behavior for the majority of the interaction. Nevertheless, in the late stages, vofTwoPhase-CentralFoam appears closer to the experimental findings. This behavior could indicate a different calculation of the vortical structures in the wake of the first cylinder.

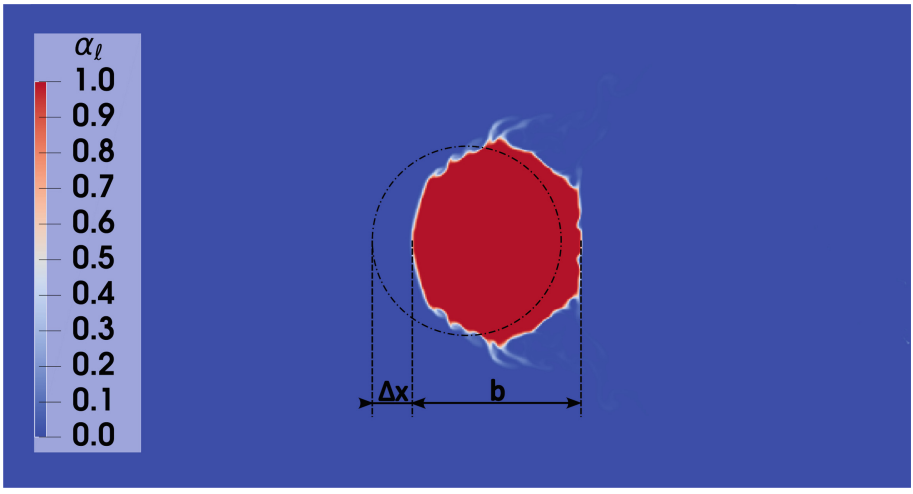

Fig. 5. Leading edge displacement and streamwise extent of the front column shown at $t^* \approx 4$ (ECOGEN).

The numerical results are further analyzed in terms of leading edge drift Δx_{LE} and streamwise deformation b, shown in Fig. 5. Both quantities are then

non-dimensionalized by the characteristic length of this problem, namely d_0, and plotted with respect to the normalized time (using the so-called *inertial* time scale), defined as follows

$$t^* = \frac{u_2}{d_0}(t - t_0), \tag{21}$$

where t_0 is the instant of the impact between the shock and the front column. Figure 6 shows the time evolution of such quantities, sampled for both solvers and compared to experimental findings by Igra and Takayama [18].

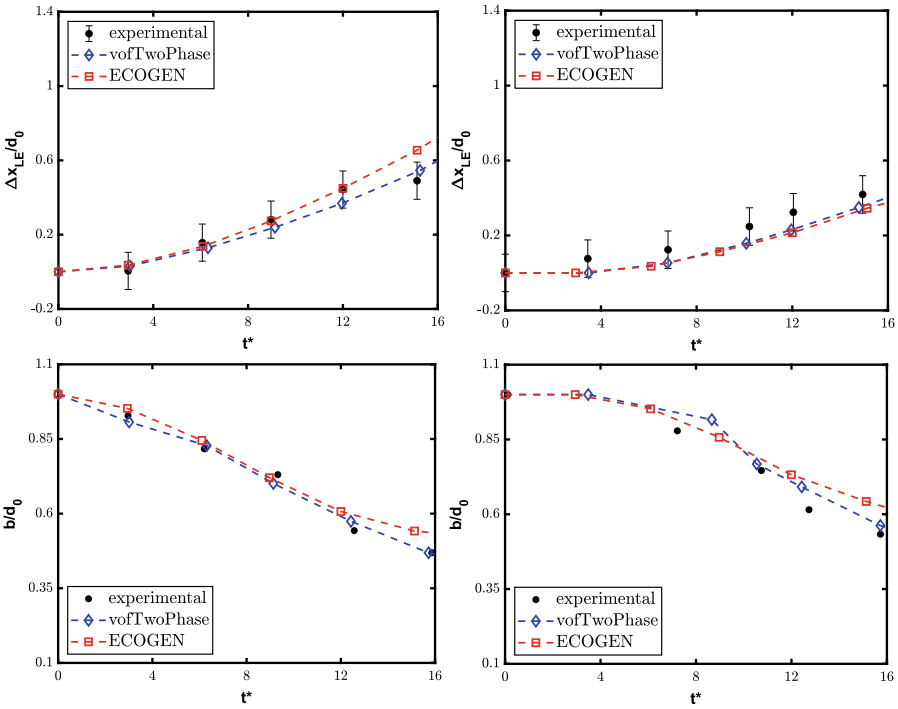

Fig. 6. Normalized leading edge displacement (top) and streamwise extent (bottom) for the front (left) and the rear column (right).

In particular, it is clear that the second column experiences less force from the air stream, as a result of the front column acting as an attenuator. As noted before, this qualitative observation is substantiated here: the surface crests on the front column, which do not undergo deformation in the late stages, make the streamwise extent less close to the experimental observations when it comes to ECOGEN. The prediction of vofTwoPhaseCentralFoam is closer as a consequence of the presence of the central trough between the two crests, as highlighted in Figs. 4 (g) and 4 (h).

5 Conclusions

Two novel open-source codes were compared, numerically reproducing the interaction between a traveling shock wave and two water columns in tandem, while simulating a shock tube device. The system of partial differential equations that govern the physical phenomenon was solved by using the FV method, supplied with high-order numerical schemes. The inevitable numerical dissipation that comes as a counterpart showed in the time evolutions of the leading edge drift and streamwise displacement. However, the complex flow field was replicated with good agreement by both codes.

Unlike previous similar works, the current research employs non-commercial softwares that allow full code access. The results of the present simulations, taking into account capillary and viscous effects, highlight the importance of these effects in modeling the late stages of shock-induced liquid fragmentation, which can improve the predictive capability of numerical solvers in practical engineering applications, such as the detonation of air-fuel mixtures. Although both ECOGEN and vofTwoPhaseCentralFoam have been shown to effectively capture primary breakup mechanisms, differences in instability formation and ligament shedding are observed, which suggests further research. In fact, while early-stage accuracy benefits from numerical dissipation, late-stage accuracy requires a more balanced treatment of interface sharpening and numerical diffusion. In this very challenging context, where a very broad range of scales play an important role, computational efficiency remains a great challenge. The use of adaptive meshing refinement strategies and the correct implementation of non-reflective boundary conditions largely decreased computational costs in terms of simulation times.

The aerobreakup of liquid droplets is an active area of research. Future work could explore the inclusion of explicit subgrid-scale models to better resolve small-scale instabilities and phenomena associated with droplet breakup [15].

Acknowledgments. The authors acknowledge financial support under the National Recovery and Resilience Plan (NRRP), Mission 4, Component 2, Investment 1.1, Call for tender No. 104 published on 2.2.2022 by the Italian Ministry of University and Research (MUR), funded by the European Union - NextGenerationEU- Project 2022B2X937 Title “Next Generation Space Propulsion Design Techniques” - CUP E53D23003080006 - Grant Assignment Decree No. 961 adopted on 30.6.2023 by MUR.

Disclosure of Interests. The authors have no competing interests to declare that are relevant to the content of this article.

References

1. Redding, J.P., Khare, P.: A computational study on shock induced deformation, fragmentation and vaporization of volatile liquid fuel droplets. Int. J. Heat Mass Transf. **184**, 122345 (2022)
2. Villermaux, E.: Fragmentation. Annu. Rev. Fluid Mech. **39**, 419–446 (2007)
3. Villermaux, E., Bossa, B.: Single-drop fragmentation determines size distribution of raindrops. Nat. Phys. **5**, 697–702 (2009)

4. Theofanous, T.G., Li, G.J.: On the physics of aerobreakup. Phys. Fluids **20**, 052103 (2008)
5. Theofanous, T.G.: Aerobreakup of Newtonian and viscoelastic liquids. Annu. Rev. Fluid Mech. **43**, 661–690 (2011)
6. Sharma, S., Chandra, N.K., Basu, S., Kumar, A.: Advances in droplet aerobreakup. Eur. Phys. J. Spec. Top. **232**, 719–733 (2023)
7. https://code-mphi.github.io/ECOGEN/. Accessed 25 Feb 2025
8. https://github.com/mkraposhin/hybridCentralSolvers/tree/edo-problem. Accessed 18 Jan 2025
9. Schmidmayer, K., Petitpas, F., Le Martelot, S., Daniel, E.: ECOGEN: an open-source tool for multiphase, compressible, multiphysics flows. Comput. Phys. Commun. **251**, 107093 (2020)
10. Kraposhin, M.V., Kukharskii, A.V., Korchagova, V.N., Shevelev, A.A.: An extension of the all-Mach number pressure-based solution framework for numerical modelling of two-phase flows with interface. Ind. Processes Technol. **166**, 6–27 (2022)
11. Rossano, V., De Stefano, G.: Computational evaluation of shock wave interaction with a cylindrical water column. Appl. Sci. **11**, 4934 (2021)
12. Rossano, V., Cittadini, A., De Stefano, G.: Computational evaluation of shock wave interaction with a liquid droplet. Appl. Sci. **12**, 1349 (2022)
13. Rossano, V., De Stefano, G.: Hybrid VOF-lagrangian CFD modeling of droplet aerobreakup. Appl. Sci. **12**, 8302 (2022)
14. Rossano, V., De Stefano, G.: Scale-resolving simulation of shock-induced aerobreakup of water droplet. Computation **12**, 71 (2024)
15. Rossano, V., De Stefano, G.: Large-eddy simulation of droplet deformation and fragmentation under shock wave impact. Appl. Sci. **15**, 1233 (2025)
16. De Stefano, G.: Wavelet-based adaptive implicit large-eddy simulation of turbulent channel flow. Comput. Fluids **272**, 106190 (2024)
17. Igra, D., Takayama, K.: Investigation of aerodynamic breakup of a cylindrical water droplet. At. Sprays **11**, 167–185 (2001)
18. Igra, D., Takayama, K.: Experimental investigation of two cylindrical water columns subjected to planar shock wave loading. J. Fluids Eng. **125**, 325–331 (2003)
19. Baer, M.R., Nunziato, J.W.: A two-phase mixture theory for the deflagration-to-detonation transition (DDT) in reactive granular materials. Int. J. Multiph. Flow **12**, 861–889 (1986)
20. Schmidmayer, K., Cazé, J., Petitpas, F., Daniel, E., Favrie, N.: Modelling interactions between waves and diffused interfaces. Int. J. Numer. Meth. Fluids **95**, 215–241 (2023)
21. Saurel, R., Petitpas, F., Berry, R.A.: Simple and efficient relaxation methods for interfaces separating compressible fluids, cavitating flows and shocks in multiphase mixtures. J. Comput. Phys. **228**, 1678–1712 (2009)
22. Biasiori-Poulanges, L., Schmidmayer, K.: A phenomenological analysis of droplet shock-induced cavitation using a multiphase modeling approach. Phys. Fluids **35**, 013312 (2023)
23. Kapila, A.K., Menikoff, R., Bdzil, J.B., Son, S.F., Stewart, D.S.: Two-phase modeling of deflagration-to-detonation transition in granular materials: reduced equations. Phys. Fluids **13**, 3002–3024 (2001)
24. Saurel, R., Pantano, C.: Diffuse-interface capturing methods for compressible two-phase flows. Annu. Rev. Fluid Mech. **50**, 105–130 (2018)
25. Meng, J.C., Colonius, T.: Numerical simulations of the early stages of high-speed droplet breakup. Shock Waves **25**, 399–414 (2015)

26. Meng, J.C., Colonius, T.: Numerical simulation of the aerobreakup of a water droplet. J. Fluid Mech. **835**, 1108–1135 (2018)
27. Dorschner, B., Biasiori-Poulanges, L., Schmidmayer, K., El-Rabii, H., Colonius, T.: On the formation and recurrent shedding of ligaments in droplet aerobreakup. J. Fluid Mech. **904**, A20 (2020)
28. Hong, Z.Y., et al.: Deformation and mutual influence of two cylindrical water columns in tandem subjected to shock wave. Chinese Phys. B **33**, 084702 (2024)
29. Schmidmayer, K., Petitpas, F., Daniel, E.: Adaptive mesh refinement algorithm based on dual trees for cells and faces for multiphase compressible flows. J. Comput. Phys. **388**, 252–278 (2019)
30. Taglialatela, F.E., De Stefano, G.: Numerical investigation of cylindrical water droplets subjected to air shock loading at a high Weber number. Fluids **10**, 81 (2025)
31. Poplavski, S.V., Minakov, A.V., Shebeleva, A.A., Boyko, V.M.: On the interaction of water droplet with a shock wave: experiment and numerical simulation. Int. J. Multiph. Flow **127**, 103273 (2020)